

Electrical Control of Single Photon Emitters in WSe₂ on a Si Nanopyramid Array with a Negligible Stark Effect

Satyabrat Behera,^{||} Jong Sung Moon,^{||} Kirlie Iulius Figuera Michal, Jaesung Heo, Jaehyun Lee, Joon-Mo Yang, Je-Hyung Kim,^{*} and Seon Namgung^{*}



Cite This: <https://doi.org/10.1021/acs.nanolett.5c05425>



Read Online

ACCESS |

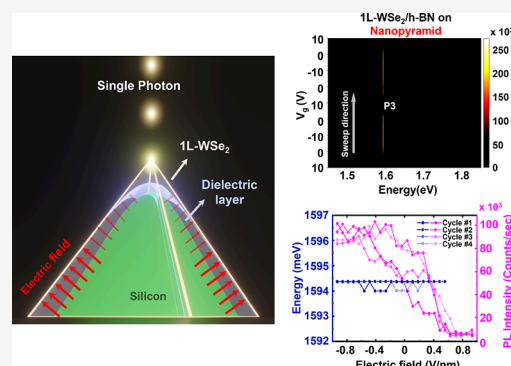
Metrics & More

Article Recommendations

Supporting Information

ABSTRACT: Single-photon emitters (SPEs) based on two-dimensional (2D) materials have attracted a lot of attention due to their unique benefits such as mechanical flexibility, high quantum yield, and easy integration on a chip. However, the electrical modulation of such emitters at a single-photon level still remains a challenge. Herein, we provide a new route to engineer electrically controllable purified SPEs in a monolayer (1L) WSe₂ using a Si nanopyramid structure. The Si nanopyramid structures allow not only the generation of high strain to localize the SPEs but also the application of voltage for electrical modulation. Of particular interest, while our structure modulates the single-photon emission with an applied gate voltage, it does not exhibit unwanted spectral shift for the applied voltage, i.e., a negligible Stark effect, due to the existence of an air gap between the 1L-WSe₂ and the nanopyramid. The single photon purity is improved by electrical modulation down to $g^{(2)}(0) = 0.06 \pm 0.03$.

KEYWORDS: Single photon emitter, Tungsten diselenide, Si nanopyramid array, Electrical control, Stark effect



The growing interest in the development of quantum communication networks and optical quantum sensors demands essential quantum-photonics building blocks such as single photon emitters (SPEs). Even though laser attenuation and the nonlinear frequency conversion method are predominantly used to generate single photons, quantum emitters have attracted lots of attention as SPEs due to guaranteed production of a single photon at a time and easy integration on a chip.^{1–3} While semiconducting quantum defects, quantum dots, and quantum well structures have been extensively studied for SPEs, recently, 2-dimensional (2D) materials have emerged as novel SPEs offering advantages such as high single-photon purity,^{4–8} easy photon extraction, mechanical flexibility,⁹ and easy integration on a chip.¹⁰ The relatively easy modulation of the 2D material-based SPEs by external stimuli such as electric field,¹¹ electrostatic doping,^{12,13} strain,^{14,15} and magnetic field¹⁶ make them strong candidates for applications in quantum information technology. The SPEs can be deterministically created by applying localized strain to 2D materials, taking advantage of both mechanical flexibility and strain-induced funneling of excitons in the 2D materials.^{6,17} While high-purity and bright single-photon emitters have been demonstrated in various 2D materials, efficient (i.e., low bias) and deterministic electrical control of individual emitters remains a major challenge. In previous approaches using nanoindentation¹⁸ and nanoposts,¹⁷ they rely on thick insulating layers or complex gate stacks,

which require high bias voltages and introduce spectral shifts. This limits wavelength-matching conditions to optical cavities, interference between remote emitters, and scalable multi-emitter operation, where spectral alignment is essential. Herein, we experimentally demonstrate efficient electrical control of purified SPEs in 1L-WSe₂ using thin dielectric layers with a negligible Stark effect deterministically created on Si nanopyramid arrays. The nanopyramids are covered with an Al₂O₃ layer using the atomic layer deposition (ALD) method, which works as a uniform high-k gate dielectric layer for electrical control. The radius curvature of the 1L-WSe₂ transferred on top of a nanopyramid is observed to be less than 10 nm, sufficient to create SPEs with high strain at the apex. These SPEs are further purified to remove the unwanted broad background defect bands by using an h-BN flake, and the emission intensity is increased as well. Not only for the deterministic formation of SPEs on it, the Si nanopyramid is also used as a gate electrode for the application of voltage to control the switching on-and-off of the SPEs. Of particular interest, the electric field on the nanopyramid structure is

Received: October 29, 2025

Revised: March 5, 2026

Accepted: March 6, 2026

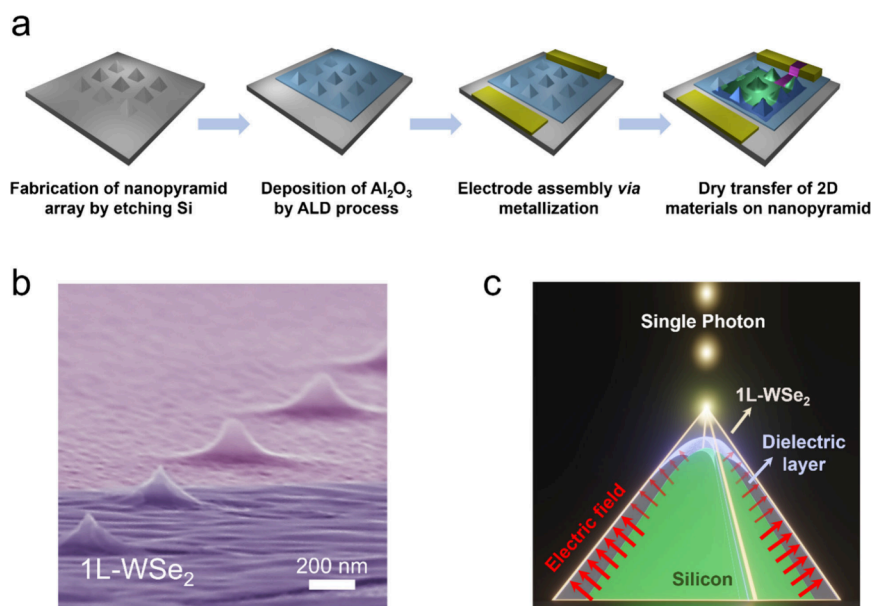


Figure 1. Strain induced single photon emitters (SPEs) on a Si nanopyramid array. (a) Fabrication process of a Si nanopyramid array. (b) FESEM image of the Si nanopyramid array covered with 1L-WSe₂. The tip apex is sharper with 1L-WSe₂, indicating the existence of an air gap between the Si nanopyramid tip and the 1L-WSe₂. (c) Schematic diagram showing the electric field distribution in 1L-WSe₂ on a Si nanopyramid. The electric field at the tip apex is lower than that on the sides due to the curvature and the existence of the air gap, leading to a negligible Stark effect during the electrical modulation of SPEs.

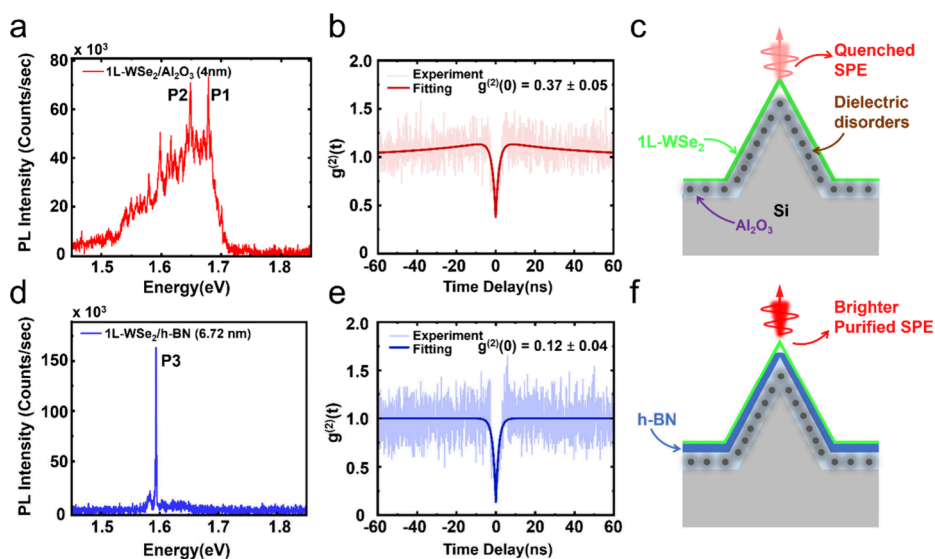


Figure 2. Characterization of SPEs in 1L-WSe₂ on an Al₂O₃-deposited Si nanopyramid array with and without h-BN. (a) Photoluminescence (PL) spectrum of 1L-WSe₂ on an Al₂O₃ (4 nm)-deposited Si nanopyramid tip apex. (b) Second-order correlation function $g^{(2)}(\tau)$ recorded from the 1L-WSe₂ on the Al₂O₃-deposited Si nanopyramid tip region showing $g^{(2)}(0)$ to be 0.37 ± 0.05 , indicative of single photon emission. (c) Schematic diagram showing the quenching of SPEs on an Al₂O₃-deposited Si nanopyramid array due to dielectric disorders in the Al₂O₃ layer. (d) Isolated PL spectrum of 1L-WSe₂ on an h-BN (6.72 nm)/Al₂O₃ (4 nm)-deposited Si nanopyramid tip apex. (e) Second-order correlation function $g^{(2)}(\tau)$ recorded from the isolated peak (P3) showing the $g^{(2)}(0)$ value to be 0.12 ± 0.05 , indicating the improved purity of SPE. (f) Schematic diagram showing the effect of the h-BN layer to prevent the interaction of dielectric disorders with SPEs. The h-BN layer eventually improves the quality of SPEs.

nonuniformly distributed, different from that on a planar structure. The electric field on the apex is ~ 20 times smaller than that on the nanopyramid-side region, which significantly reduces and, in some cases, eliminates the shift of photon energy of SPEs, i.e., a negligible Stark effect. The immunity of the nanopyramid structure to externally applied voltage should presumably protect the SPEs from unwanted change of the photon energy caused by the instability such as charge trapping

at gate dielectric layers during multiple gate operation,¹⁹ noisy fluctuation of the gate voltage in complex integrated circuits,²⁰ and electric field fluctuations inherent to the microenvironment.²¹ Our pyramidal-tip-based device enables low-voltage, high-contrast intensity modulation with a simple configuration while preserving spectral stability across the entire gating range. This allows the emitter intensity to be modulated independently of emission energy, which is critical for cavity-

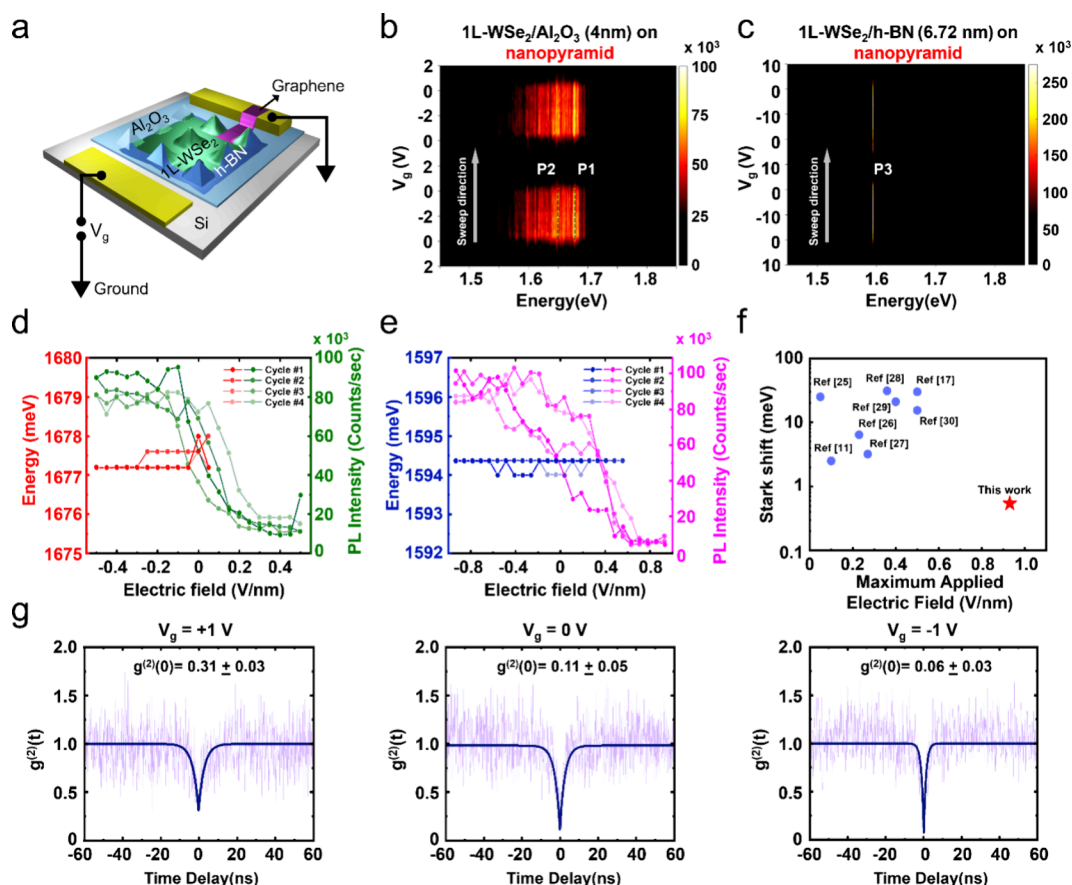


Figure 3. Stark effect free modulation of SPEs in 1L-WSe₂ on Si nanopyramid arrays. (a) Schematic diagram of an electrically switchable SPE device. Voltage modulation of PL spectra of SPE in 1L-WSe₂ (b) without h-BN and (c) with a 6.72 nm thick h-BN layer. A 4 nm Al₂O₃ layer is deposited on top of Si nanopyramid arrays for both cases. (d, e) Corresponding plot of photon energy (left, showing negligible Stark shift) and PL intensity (right) for P1 in (b) and the P3 peak in (c), respectively. The SPE peaks exhibit unconventional negligible Stark shifts while modulating the PL intensity. (f) Comparison of the Stark shift of SPEs observed in our work (red solid star) with those in other references (blue solid circles). The Stark shift in our case is significantly lower than those in other references. (g) Measured second order photon-correlation at different gate voltages. Enhancement in the single photon purity is observed in the negative gate voltage.

coupled devices and for scalable quantum photonic architectures requiring independent electrical control of multiple emitters. Furthermore, because our Si nanopyramid arrays are fabricated from etching a Si wafer, it should be advantageous for the integration with conventional well-developed Si optoelectronic components, facilitating the practical application of SPEs for chip-based quantum communication, photonic quantum computing, and quantum optical sensors.

Figure 1a schematically demonstrates the fabrication process of the SPE devices used in this work. First, Si nanopyramid arrays are fabricated via an etching process²² (see [method section](#) for detailed fabrication process). A 4 nm Al₂O₃ layer as a gate dielectric for an electrical control is deposited on the nanopyramid array via ALD, and 1L-WSe₂ and a few-layer graphene flakes are transferred on the nanopyramid array via the polypropylene carbonate (PPC)-based stamping process as described in the [method section](#). Figure 1b shows a false-colored field emission scanning electron microscope (FESEM) image showing the side-view of the nanopyramid array partially covered with 1L-WSe₂. The FESEM image reveals the heights and widths of nanopyramid as around 200 and 300 nm, respectively. Of note, 1L-WSe₂ covering the nanopyramid (purple-colored area) forms a sharply pointed apex on top of the nanopyramid tip, distinctly from the rather rounded apex

of the uncovered nanopyramid (pink-colored area). The radius of curvature of the uncovered Si nanopyramid varies between ~20 and ~80 nm. On the other hand, the radius of curvature of the 2D materials on the tip is less than 10 nm as shown in Figure 1b and [Supporting Information Figure S1](#), which is small enough to induce high strain on the flake required for the creation of SPEs. The different radius of curvature of the apex depending on the existence of 1L-WSe₂ indicates the separation of 1L-WSe₂ from the nanopyramid tip with an air gap, which is schematically illustrated in Figure 1c. The DC electric field between 1L-WSe₂ and a Si nanopyramid with applied voltage varies dominantly depending on its proximity with the nanopyramid, and therefore, the electric field decreases approaching the apex (Figure 1c).

A photoluminescence (PL) spectrum was acquired from the nanopyramid region at 4 K with a 532 nm continuous-wave laser (see the [method section](#) for detailed optical setup). The PL spectrum is shown in Figure 2a, which exhibits two prominent peaks at 1.678 eV (P1) and at 1.650 eV (P2) overlapping with broader defect bands. These sharp peaks are ascribed to the high strain at the tip apex of the nanopyramid.²³ To check the single-photon characteristic of the observed emission peaks, we spectrally filtered the peak and performed a second-order photon-correlation measurement $g^{(2)}(\tau)$ using a standard Hanbury-Brown and Twiss setup. As

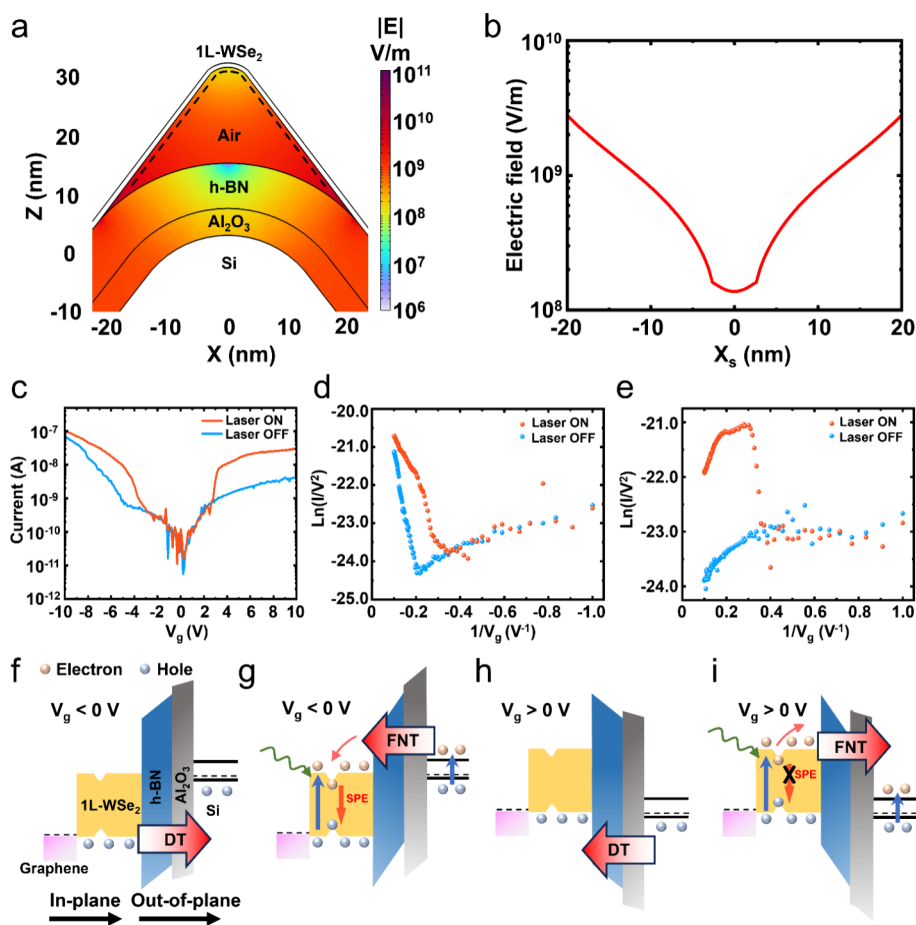


Figure 4. Mechanism of a negligible Stark effect and electrical modulation of an SPE. (a) Cross-section of simulated DC electric field distribution in the region between 1L-WSe₂ and a Si nanopyramid tip. Here, we used 4 nm radius curvature of the tip. (b) Electric field in 1L-WSe₂ along the dashed line denoted in (a). (c) I - V data of the SPE device for laser-on (red) and -off (blue) cases. Fowler-Nordheim tunneling plot for the laser-on case in the (d) negative and (e) positive gate voltages, respectively. Schematic diagram explaining the charge transport mechanism across the dielectric layer for (f, g) negative and (h, i) positive gate voltage, with laser-off and -on, respectively. FNT and DT denote Fowler-Nordheim tunneling and direct tunneling, respectively.

shown in Figure 2b, photon antibunching is observed with $g^{(2)}(0) = 0.37 \pm 0.05$, which is below the threshold of 0.5, indicative of a single photon source. Even though the observed peaks in the spectrum exhibit photon antibunching (Figure 2b), the intensity of the peak is not overwhelming compared to that of the background defect signal, and the purity of single photons remain limited. The relatively low intensity of SPE peaks is attributed to the disorders of Al₂O₃ layer, such as dangling bonds, vacancy, and impurities in the Al₂O₃ layer, which trap charges to reduce the radiative recombination²⁴ (Figure 2c).

To block the unwanted quenching and relaxation from the Al₂O₃ dielectric layer, we transferred a few-layer h-BN on top of the Al₂O₃ dielectric layer. We observed stronger PL intensity on the tip apex of nanopyramids, indicating the deterministic creation of SPEs on top of the nanopyramid array (Supporting Information Figure S2a). The PL spectrum from the point exhibiting the strong intensity shows a narrow isolated PL emission peak at 1.594 eV (P3), which dominates the spectrum (Figure 2d). The second-order photon-correlation measurement (Figure 2e) performed on this peak exhibits photon antibunching with $g^{(2)}(0) = 0.12 \pm 0.04$, indicating an SPE. In addition, the peak shows a brightness of 1.09 ± 0.08 MHz, one of the representative properties of SPEs (Supporting

Information Figure S2b). Also, in Supporting Information Figure S2c, we show a higher brightness of 10.11 ± 0.73 MHz from the other SPE. As schematically shown in Figure 2f, the added h-BN flake serves as a barrier to isolate SPEs in 1L-WSe₂ from the disorders in the Al₂O₃ layer, resulting in spectral isolation of the SPE peak with the suppression of the broad background. Such an isolation from the disorder leads to a noticeably ~ 3 times lower $g^{(2)}(0)$ value than that of the Al₂O₃-only case (Figures 2b and 2e). These results indicate that the SPEs on the few-layer-thick h-BN on Si nanopyramid arrays generate single photons with significantly improved purity and brightness.

To study the electrical controllability of the SPEs on our nanostructures, a gate voltage was applied to the 1L-WSe₂ through Si nanopyramid arrays as shown in the schematics of Figure 3a. For the case in which only Al₂O₃ was used as a gate dielectric layer, we observed the single photon emission peaks (both P1 and P2) and broad defect bands turning on with gate voltage $V_g < 0.4$ V as shown in Figure 3b. For the case of the 6.72 nm thick h-BN covering Al₂O₃, we also observed a similar trend, in which the SPE turned on for a negative gate voltage (Figure 3c). The intensity profiles along the applied electric field for both devices are shown in greenish solid lines in Figure 3d and pinkish solid lines in Figure 3e, and the SPEs are

switched on and off within 2 and 13 V, respectively. Thus, the deterministically created SPEs on our Si nanopyramid structures can be controlled in an electrical manner with simple gate structures within a small voltage range.

Of particular interest, the photon energy shift along the applied voltage, i.e., Stark shift, is restricted to less than 1 meV for the case of the SPE on the only Al_2O_3 layer (P1, reddish solid lines in Figure 3d), while no Stark shift is observed within our spectral resolution for the case of the SPE on the h-BN/ Al_2O_3 case (P3, bluish solid line in Figure 3e). We consistently observed the negligible Stark effect for other SPEs while the intensity was modulated with an applied electric field (Supporting Information Figure S3). Our work shows the lowest Stark shift of 0.54 meV at a maximum applied electric field of 0.93 V/nm, which is surprisingly small compared to other references^{11,17,25–30} even with a higher electric field as shown in Figure 3f. We also note the $g^2(0)$ value indicating single photon purity was enhanced to 0.06 ± 0.03 with negative gate voltage (Figure 3g), comparable to that of recently reported chemically functionalized, voltage-treated, and nanogap-coupled WSe_2 ,^{31–33} which is attributed to the increased single photon emission relative to background noise at negative gate voltage.¹⁸

To understand the mechanism for the negligible Stark shift observed in our system, we calculate the DC electric field around a 1L- WSe_2 apex in a three-dimensional 1L- WSe_2 /h-BN/nanopyramid structure model using a simulation based on the finite element method (FEM) in COMSOL Multiphysics 6.1. A detailed description of the simulation is presented in the Methods section. The cross-sectional distribution of the DC electric field around the 1L- WSe_2 apex at $V_g = 10$ V, mimicking the experimental condition for P3, is shown in Figure 4a. The DC electric field at the apex is lower compared to that at the sidewall by ~ 20 times. The variation of the induced electric field along the 1L- WSe_2 slope (dashed line in Figure 4a) clearly shows an electric field minimum formed at the apex (Figure 4b). The electric field between two layers is nonuniform on curved structures, in contrast to the uniform electric field on flat planar structures. Furthermore, the air gap formed between 1L- WSe_2 and a h-BN, as stated earlier in Figure 1b and 1c, induces different electric fields depending on the distance from the nearest point of the Si nanopyramid held with the same gate voltage. As a result, the electric field applied on 1L- WSe_2 on a Si nanopyramid structure is not uniform, and the electric field at the apex is small compared to the flat side-wall region. Due to the small electric field with given gate voltage, the Stark effect is suppressed at the apex, where SPEs are selectively created with high strain. We also performed control experiments on a different sample with a 28 nm thick h-BN, where a 1L- WSe_2 /h-BN heterostructure is suspended over a Si nanopyramid array in an almost flattened form without any sharp curvature in WSe_2 (Supporting Information Figure S4). In the case of the 28 nm thick h-BN, the effective high strain on the 1L- WSe_2 almost disappears, and therefore, the PL spectrum is devoid of sharp peaks indicating SPEs. Contrary to the previous case, we observed a 15.0 meV energy shift in the PL spectrum at a maximum electric field of 0.60 V/nm (Supporting Information Figure S4c), and the DC electric field on the 1L- WSe_2 is uniformly distributed as shown in the simulation data (Supporting Information Figure S4d). All these results indicate that the sharp geometry of 1L- WSe_2 on a Si nanopyramid tip with an air gap induces a nonuniform electric field and minimizes the Stark shift of SPEs. In comparison,

previous approaches for electrical control of SPEs quite differ from our approach in that it uses planar gate electrode structures parallel to 2D materials possessing SPEs.^{17,26,34} For example, a graphene sheet for a gate electrode and an h-BN sheet for a gate dielectric layer are stacked in parallel with a TMDC layer possessing SPEs for electrical control. In such cases, the electric field should be almost uniform over the whole planar region due to the same distance between a graphene sheet and a TMDC layer possessing SPEs. Even in cases where the heterostructures of the TMDC/h-BN/graphene structure are transferred on top of nanostructures, such as nanopillars for deterministic creation of SPEs, the two layers are still parallel without an air gap. In this case, the electric field is quite uniform without a suppressed electric field at the tip as seen in our approach (Figures 4a,b). Thus, our approach using a Si nanopyramid offers a distinct and effective way to engineer a reduced electric field on the apex, leading to the suppression of the Stark effect. Thus, by employing the engineered negligible Stark effect using our Si nanopyramid structure, we can fabricate SPEs that are stable against external noisy environments such as time-variant charge distribution at the gate dielectric and noisy gate operations.

To explain the tunability of SPEs albeit with the negligible Stark effect, we analyze the I - V data of the devices (Figure 4c-e) and provide a charge transport mechanism for the devices (Figure 4f-i). Since our experiments are performed at low temperature (4 K), holes are dominant charge carriers in our devices with p -type 1L- WSe_2 and Si, and charge carrier transport is governed by a tunneling mechanism rather than thermionic emission. For the negative V_g without laser illumination, a transition is observed at -5 V in the Fowler-Nordheim (FN) plot (blue dots in Figure 4d), which indicates a direct tunneling for -5 V $< V_g < 0$ V and FN tunneling for -10 V $< V_g < -5$ V. Considering the given negative V_g and p -type dopants, the observed tunneling is attributed to the holes in 1L- WSe_2 tunneling toward the Si electrode as shown in Figure 4f. On the other hand, for the negative V_g with laser illumination, a transition from direct to FN tunneling is observed at a lower $V_g = -2.9$ V in the FN plot (red dot in Figure 4d) with increased tunneling current for $V_g < -2.9$ V compared to the laser-off case. The shift of the transition voltage and the increased current is attributed to the tunneling of photoexcited electrons of Si with a lowered tunneling barrier for the photoexcited electrons^{35,36} (Figure 4g; Supporting Information Section S5). The electrons in the 1L- WSe_2 tunnel and recombine at the nanopyramid tip to generate single photons (Figure 3c and 4g). For the positive V_g without laser illumination, holes in Si tunnel through the dielectric barriers of Al_2O_3 and h-BN toward the 1L- WSe_2 via direct tunneling as shown in Figure 4h. For the positive V_g with laser illumination, a transition from direct to FN tunneling is observed at 2.6 V, which is attributed to the tunneling of photoexcited electrons generated in 1L- WSe_2 (red dots in Figure 4e). The FN tunneling of photoexcited electrons from 1L- WSe_2 to Si results in the increase of the current at $V_g = 2.6$ V (Figure 4i). Of note, this transition voltage is the same with the turn-off voltage of SPE (Figure 3c), which further confirms that the FN tunneling of electrons from 1L- WSe_2 to Si suppresses the SPE at the nanopyramid tip. The nonlinear behavior beyond 3.6 V in Figure 4e is presumably attributed to an insufficient carrier supply.³⁷ The measured current shown in Figure 4c-4e explains reasonably the electron tunneling with and without the excitation laser and the occupation of charge carriers in the

single photon emitter. However, all the current measured in the graphs does not contribute to the occupation of the single photon emitters. Given the large laser spot size of $\sim 1 \mu\text{m}$ compared to the single photon emitter size of $\sim 2 \text{ nm}$,³⁴ most of the measured tunneling current occurs out of the single photon emitter. Even considering the nanosecond scale of lifetime of radiative and nonradiative recombination rate of the single photon emitter, 0.1 nA current is enough to occupy a single photon emitter even assuming full occupation. Thus, while the proposed mechanism explains the intensity control of a single photon emitter, the large current change during the tunneling transition does not appear as a corresponding change in the PL intensity. Rather, the PL intensity exhibits gradual change as mentioned in the previous reports.^{17,29,34} We fit the PL intensity change based on sigmoid and logistic functions³⁴ and measured switching voltage as 2.42 and 2.79 V, respectively. This mechanism also explains the observed hysteresis of the PL signals during the repetitive sweeps shown in Figure 3e and S6a, where voltage sweeps from 10 V to -10 V are denoted by odd-numbered cycles and voltage sweeps from -10 to 10 V are denoted by even-numbered cycles. After the odd-numbered sweep (i.e., toward negative V_g), the electron traps in the interface between layers or intrinsic traps in 1L-WSe₂ are more likely to be occupied due to electron tunneling from Si (Figure 4g). The electron charging in the traps increases the PL signal in the given system, thereby leading to higher PL signals in the following even-numbered sweep and resulting in the hysteresis.

In conclusion, we demonstrate a novel approach to electrically control purified SPEs in 1L-WSe₂ using a Si nanopyramid array. The sharp Si nanopyramid structure allows not only induction of strong local strain in 1L-WSe₂ to create and localize SPEs but also application of gate voltage to the WSe₂ layer for electrical control. A few-layer h-BN is used to remove the broad background defect bands leading to an increase in the single-photon purity and the intensity of SPEs while preserving the small radius of curvature of the 1L-WSe₂ (less than 10 nm) at the apex to create and localize the SPEs on the nanopyramid. We also demonstrate that the SPEs on Si nanopyramid arrays can be efficiently controlled by applying a gate voltage to 1L-WSe₂. The inclusion of an additional tunneling path of FN tunneling at high gate voltage reduces the photogenerated charge density in 1L-WSe₂ quenching the SPE. More interestingly, the negligible Stark shift is observed for the SPEs on the Si nanopyramid arrays, which is attributed to the curved structure of our platform and the formation of air gap inside. The proposed strategy to purify SPEs in 2D materials and simultaneously control them via an external gate voltage on Si nanopyramid arrays will pave a new way to develop compact on-chip devices for quantum communication, computing, and sensing, compatible with matured Si-based optoelectronic technology.

1. FABRICATION OF SPE DEVICES

Starting with a 90 nm SiO₂/Si wafer, a 90 nm SiO₂ layer was etched using dielectric reactive ion etching for a square region defined by photolithography. We patterned gate electrodes by additional photolithography and metal evaporation of Au (50 nm)/Ti (5 nm). We patterned nanosquare arrays of $300 \times 300 \text{ nm}$ on the exposed Si region using electron-beam lithography followed by chromium metal deposition. Inductively coupled plasma reactive ion etching was performed to create the nanopyramid-shaped structure on the Si region. We deposited

4 nm Al₂O₃ using an atomic layer deposition process. For defining top electrodes, we deposited Au(50 nm)/Ti(5 nm) after additional photolithography process.

2. TRANSFER OF 1L-WSE₂, H-BN, AND FEW-LAYER GRAPHENE ON AN SPE DEVICE

1L-WSe₂, h-BN, and few-layer graphene were exfoliated on a 90 nm SiO₂/Si substrate from commercial bulk crystals (HQ Graphene Company). A polypropylene/polydimethylpolysiloxane (PPC/PDMS) stamp was brought in contact with few-layer graphene using a micromanipulator and heated to 40 °C. The stamp was released slowly after being cooled to 30 °C to pick up the few-layer graphene. The same process was repeated to pick up 1L-WSe₂ and few-layer h-BN flakes to make a 1L-WSe₂/h-BN/graphene heterostack on a PPC/PDMS stamp. The heterostack was aligned and brought in close contact with the nanopyramid array. The sample stage was heated to 120 °C, and the micromanipulator was slowly retracted to release the heterostack on the nanopyramid array. Finally, the sample was connected to the sample holder pad via wire bonding technique for voltage-dependent PL measurement.

3. OPTICAL SETUP

The fabricated device was mounted on a 4 K closed-cycle cryostat with low vibration and then excited by a 532 nm continuous-wave pump laser. We focused the excitation beam and collected the optical signals from the device using a high-NA objective lens (100 \times , NA = 0.7). For wide-field luminescence imaging, the laser spot size was enlarged to $\sim 500 \mu\text{m}^2$, and the emission was sent to the charge-coupled device. To characterize the spectrum of the emission from the device, we used a 700 nm long-pass filter to spectrally filter out the pump laser and then sent the resolved emission to a spectrometer with a spectral resolution of 0.03 nm, installed with a nitrogen-cooled 2D array charge-coupled device (CCD). To characterize the single photon nature of the emission, we sent the resolved emission from the spectrometer to a Hanbury Brown and Twiss interferometer composed of a 50:50 beamsplitter and two silicon avalanche photodiodes connected to time-correlated single photon counting. The measured second-order photon correlation was fitted by eq 1 considering an instrument response function of a Gaussian function with a full width at half-maximum of 225 ps, which is restricted by the avalanche photodiode.

$$g^{(2)}(\tau) = 1 - (1 - g^{(2)}(0))e^{-|\tau|/\tau_0} \quad (1)$$

where τ_0 is the mixture of the pumping and decay times of the quantum emitter.

4. NUMERICAL SIMULATION

We used finite element method (FEM) using COMSOL Multiphysics 6.1 with an AC/DC module to analyze the DC electric field within the hybrid system. The model includes 3D geometry of the 1L-WSe₂/h-BN/Al₂O₃/Si nanopyramid structure. The nanopyramid dimension in the model was set to 66 nm (height) by 100 nm (width), material properties were obtained from refs 38 and 39, and voltages were imposed to the 1L-WSe₂ and Si nanopyramid.

■ ASSOCIATED CONTENT

SI Supporting Information

The Supporting Information is available free of charge at <https://pubs.acs.org/doi/10.1021/acs.nanolett.5c05425>.

S1. FESEM characterization of the 1L-WSe₂/h-BN layer on a Si nanopillar array; S2. Characteristics of single photon emitters on 1L-WSe₂/h-BN; S3. Electrical modulation of additional single photon emitters; S4. Characterization and electrical modulation of PL emission from 1L-WSe₂ over thick h-BN on a Si nanopillar array; S5. Low tunneling barrier height for photoexcited charge carriers; S6. Determination of SPE turn-off gate voltage (PDF)

■ AUTHOR INFORMATION

Corresponding Authors

Seon Namgung – Department of Physics, Ulsan National Institute of Science and Technology (UNIST), Ulsan 44919, Republic of Korea; orcid.org/0000-0002-1730-1665; Email: seon@unist.ac.kr

Je-Hyung Kim – Department of Physics, Ulsan National Institute of Science and Technology (UNIST), Ulsan 44919, Republic of Korea; orcid.org/0000-0002-6894-9285; Email: jehyungkim@unist.ac.kr

Authors

Satyabrat Behera – Department of Physics, Ulsan National Institute of Science and Technology (UNIST), Ulsan 44919, Republic of Korea

Jong Sung Moon – Department of Physics, Ulsan National Institute of Science and Technology (UNIST), Ulsan 44919, Republic of Korea; Present Address: Quantum Technology Research Division, Electronics and Telecommunications Research Institute (ETRI), Daejeon 34129, Republic of Korea. (J.S.M.)

Kirlie Iulius Figuera Michal – Department of Physics, Ulsan National Institute of Science and Technology (UNIST), Ulsan 44919, Republic of Korea

Jaesung Heo – Department of Physics, Ulsan National Institute of Science and Technology (UNIST), Ulsan 44919, Republic of Korea; orcid.org/0009-0004-7587-5722

Jaehyun Lee – Department of Physics, Ulsan National Institute of Science and Technology (UNIST), Ulsan 44919, Republic of Korea; orcid.org/0009-0006-4179-8997

Joon-Mo Yang – Department of Biomedical Engineering, Ulsan National Institute of Science and Technology (UNIST), Ulsan 44919, Republic of Korea

Complete contact information is available at: <https://pubs.acs.org/doi/10.1021/acs.nanolett.5c05425>

Author Contributions

^{||}S.B. and J.S.M. contributed equally to the current study.

Notes

The authors declare no competing financial interest.

■ ACKNOWLEDGMENTS

This work is supported by the IITP (Institute of Information & Communications Technology Planning & Evaluation)-ITRC (Information Technology Research Center) grant funded by the Korea government (Ministry of Science and ICT, MSIT)

(IITP-2025-RS-2023-00259676). This work is also supported by the 2025 Research Fund (1.250007.01) of UNIST (Ulsan National Institute of Science & Technology), the National Research Foundation of Korea grant funded by MSIT (RS-2024-00442762 and RS-2019-NR042359), and the IITP grant funded by MSIT (RS-2024-00401037, RS-2024-00338878). This work is also partly supported by Korean-Swiss Science and Technology Programme through the National Research Foundation of Korea (NRF) (RS-2025-02308415) and Institute of Information and communications Technology Planning and Evaluation (IITP) (RS-2025-25464990, Development of an Advanced Module for High-Purity, High-Indistinguishability Single-Photon Sources and Its Application to Multi-Photon Entanglement Technologies) grant funded by MSIT. We thank UNIST Central Research Facilities (UCRF) for the support of its facilities and equipment.

■ REFERENCES

- (1) Esmann, M.; Wein, S. C.; Antón-Solanas, C. Solid-State Single-Photon Sources: Recent Advances for Novel Quantum Materials. *Adv. Funct. Mater.* **2024**, *34* (30), 2315936.
- (2) Liu, G.; Zhou, W.; Gromyko, D.; Huang, D.; Dong, Z.; Liu, R.; Zhu, J.; Liu, J.; Qiu, C.-W.; Wu, L. Single-photon generation and manipulation in quantum nanophotonics. *Applied Physics Reviews* **2025**, *12* (1), 011308.
- (3) Neumann, M.; Wei, X.; Morales-Inostroza, L.; Song, S.; Lee, S.-G.; Watanabe, K.; Taniguchi, T.; Götzinger, S.; Lee, Y. H. Organic Molecules as Origin of Visible-Range Single Photon Emission from Hexagonal Boron Nitride and Mica. *ACS Nano* **2023**, *17* (12), 11679–11691.
- (4) He, Y.-M.; Clark, G.; Schaibley, J. R.; He, Y.; Chen, M.-C.; Wei, Y.-J.; Ding, X.; Zhang, Q.; Yao, W.; Xu, X.; et al. Single quantum emitters in monolayer semiconductors. *Nat. Nanotechnol.* **2015**, *10* (6), 497–502.
- (5) Tran, T. T.; Zachreson, C.; Berhane, A. M.; Bray, K.; Sandstrom, R. G.; Li, L. H.; Taniguchi, T.; Watanabe, K.; Aharonovich, I.; Toth, M. Quantum Emission from Defects in Single-Crystalline Hexagonal Boron Nitride. *Physical Review Applied* **2016**, *5* (3), 034005.
- (6) Lee, S.-J.; Chuang, H.-J.; Yeats, A. L.; McCreary, K. M.; O'Hara, D. J.; Jonker, B. T. Ferroelectric Modulation of Quantum Emitters in Monolayer WS₂. *ACS Nano* **2024**, *18* (36), 25349–25358.
- (7) Wu, W.; Strasser, A.; Xiu, Z.; Ngan, K.; Hoang, T. D.; Liu, S.; Shen, H.; Holtzman, L. N.; Edgar, J. H.; Hone, J. C.; et al. Ultrahigh-Purity Single-Photon Emission from 2D WSe₂ via Effective Suppression of Classical Emission. *Nano Lett.* **2025**, *25* (29), 11226–11233.
- (8) Chatterjee, A.; Biswas, A.; Fuhr, A. S.; Terlier, T.; Sumpter, B. G.; Ajayan, P. M.; Aharonovich, I.; Huang, S. Room-temperature high-purity single-photon emission from carbon-doped boron nitride thin films. *Science Advances* **2025**, *11* (25), No. eadv2899.
- (9) Bertolazzi, S.; Brivio, J.; Kis, A. Stretching and Breaking of Ultrathin MoS₂. *ACS Nano* **2011**, *5* (12), 9703–9709.
- (10) Kim, S.; Fröch, J. E.; Christian, J.; Straw, M.; Bishop, J.; Totonjian, D.; Watanabe, K.; Taniguchi, T.; Toth, M.; Aharonovich, I. Photonic crystal cavities from hexagonal boron nitride. *Nat. Commun.* **2018**, *9* (1), 2623.
- (11) Noh, G.; Choi, D.; Kim, J.-H.; Im, D.-G.; Kim, Y.-H.; Seo, H.; Lee, J. Stark Tuning of Single-Photon Emitters in Hexagonal Boron Nitride. *Nano Lett.* **2018**, *18* (8), 4710–4715.
- (12) Brotons-Gisbert, M.; Branny, A.; Kumar, S.; Picard, R.; Proux, R.; Gray, M.; Burch, K. S.; Watanabe, K.; Taniguchi, T.; Gerardot, B. D. Coulomb blockade in an atomically thin quantum dot coupled to a tunable Fermi reservoir. *Nat. Nanotechnol.* **2019**, *14* (5), 442–446.
- (13) White, S. J. U.; Yang, T.; Dontschuk, N.; Li, C.; Xu, Z.-Q.; Kianinia, M.; Stacey, A.; Toth, M.; Aharonovich, I. Electrical control of quantum emitters in a Van der Waals heterostructure. *Light: Science & Applications* **2022**, *11* (1), 186.

- (14) Kim, H.; Moon, J. S.; Noh, G.; Lee, J.; Kim, J.-H. Position and Frequency Control of Strain-Induced Quantum Emitters in WSe₂ Monolayers. *Nano Lett.* **2019**, *19* (10), 7534–7539.
- (15) Iff, O.; Tedeschi, D.; Martín-Sánchez, J.; Moczala-Dusanowska, M.; Tongay, S.; Yumigeta, K.; Taboada-Gutiérrez, J.; Savaresi, M.; Rastelli, A.; Alonso-González, P.; et al. Strain-Tunable Single Photon Sources in WSe₂ Monolayers. *Nano Lett.* **2019**, *19* (10), 6931–6936.
- (16) Wang, Q.; Maisch, J.; Tang, F.; Zhao, D.; Yang, S.; Joos, R.; Portalupi, S. L.; Michler, P.; Smet, J. H. Highly Polarized Single Photons from Strain-Induced Quasi-1D Localized Excitons in WSe₂. *Nano Lett.* **2021**, *21* (17), 7175–7182.
- (17) Guo, S.; Germanis, S.; Taniguchi, T.; Watanabe, K.; Withers, F.; Luxmoore, I. J. Electrically Driven Site-Controlled Single Photon Source. *ACS Photonics* **2023**, *10* (8), 2549–2555.
- (18) Stevens, C. E.; Chuang, H.-J.; Rosenberger, M. R.; McCreary, K. M.; Dass, C. K.; Jonker, B. T.; Hendrickson, J. R. Enhancing the Purity of Deterministically Placed Quantum Emitters in Monolayer WSe₂. *ACS Nano* **2022**, *16* (12), 20956–20963.
- (19) Specht, M.; Reisinger, H.; Hofmann, F.; Schulz, T.; Landgraf, E.; Luyken, R. J.; Rösner, W.; Grieb, M.; Risch, L. Charge trapping memory structures with Al₂O₃ trapping dielectric for high-temperature applications. *Solid-State Electron.* **2005**, *49* (5), 716–720.
- (20) Lee, J. H.; Nidhi, K.; Ker, M. D. System-Level ESD-Induced Voltage Fluctuation to the Power of Integrated Circuits on System Board. *IEEE Transactions on Electromagnetic Compatibility* **2022**, *64* (6), 1883–1889.
- (21) Conradt, F.; Bezold, V.; Wiechert, V.; Huber, S.; Mecking, S.; Leitenstorfer, A.; Tenne, R. Electric-Field Fluctuations as the Cause of Spectral Instabilities in Colloidal Quantum Dots. *Nano Lett.* **2023**, *23* (21), 9753–9759.
- (22) Cheon, S.; Jeong, D. S.; Park, J.-K.; Kim, W. M.; Lee, T. S.; Lee, H.; Kim, I. Enhanced blue responses in nanostructured Si solar cells by shallow doping. *J. Phys. D: Appl. Phys.* **2018**, *51* (12), 125102.
- (23) Yang, L.; Yuan, Y.; Fu, B.; Yang, J.; Dai, D.; Shi, S.; Yan, S.; Zhu, R.; Han, X.; Li, H.; et al. Revealing broken valley symmetry of quantum emitters in WSe₂ with chiral nanocavities. *Nat. Commun.* **2023**, *14* (1), 4265.
- (24) Kim, S. Y.; Yang, H. I.; Choi, W. Photoluminescence quenching in monolayer transition metal dichalcogenides by Al₂O₃ encapsulation. *Appl. Phys. Lett.* **2018**, *113* (13), 133104.
- (25) Patel, R. B.; Bennett, A. J.; Farrer, I.; Nicoll, C. A.; Ritchie, D. A.; Shields, A. J. Two-photon interference of the emission from electrically tunable remote quantum dots. *Nat. Photonics* **2010**, *4* (9), 632–635.
- (26) Ripin, A.; Peng, R.; Zhang, X.; Chakravarthi, S.; He, M.; Xu, X.; Fu, K.-M.; Cao, T.; Li, M. Tunable phononic coupling in excitonic quantum emitters. *Nat. Nanotechnol.* **2023**, *18* (9), 1020–1026.
- (27) Zhigulin, I.; Horder, J.; Ivády, V.; White, S. J. U.; Gale, A.; Li, C.; Lobo, C. J.; Toth, M.; Aharonovich, I.; Kianinia, M. Stark Effect of Blue Quantum Emitters in Hexagonal Boron Nitride. *Physical Review Applied* **2023**, *19* (4), 044011.
- (28) Xia, Y.; Li, Q.; Kim, J.; Bao, W.; Gong, C.; Yang, S.; Wang, Y.; Zhang, X. Room-Temperature Giant Stark Effect of Single Photon Emitter in van der Waals Material. *Nano Lett.* **2019**, *19* (10), 7100–7105.
- (29) Chakraborty, C.; Goodfellow, K. M.; Dhara, S.; Yoshimura, A.; Meunier, V.; Vamivakas, A. N. Quantum-Confined Stark Effect of Individual Defects in a van der Waals Heterostructure. *Nano Lett.* **2017**, *17* (4), 2253–2258.
- (30) Nikolay, N.; Mendelson, N.; Sadzak, N.; Böhm, F.; Tran, T. T.; Sontheimer, B.; Aharonovich, I.; Benson, O. Very Large and Reversible Stark-Shift Tuning of Single Emitters in Layered Hexagonal Boron Nitride. *Physical Review Applied* **2019**, *11* (4), 041001.
- (31) Ananth, R.; Utama, M. I. B.; Xu, D. D.; Vong, A. F.; Sadhukhan, T.; Zeng, H.; López-Arteaga, R.; Wang, W.; Namgung, S. D.; Gavin, S. C.; et al. Enhanced spectral purity of WSe₂ quantum emitters via conformal organic adlayers. *Science Advances* **2025**, *11* (40), No. eady7557.
- (32) Lee, S.-J.; Chuang, H.-J.; McCreary, K. M.; Noyan, M. A.; Jonker, B. T. Voltage-Induced Degradation for Enhanced Purity and Reproducibility of Quantum Emission in Monolayer 2D Materials. *ACS Nano* **2025**, *19* (38), 33981–33990.
- (33) Cai, H.; Rasmita, A.; He, R.; Zhang, Z.; Tan, Q.; Chen, D.; Wang, N.; Mu, Z.; Eng, J. J. H.; She, Y.; et al. Charge-depletion-enhanced WSe₂ quantum emitters on gold nanogap arrays with near-unity quantum efficiency. *Nat. Photonics* **2024**, *18* (8), 842–847.
- (34) Hötger, A.; Klein, J.; Barthelmi, K.; Sigl, L.; Sigger, F.; Männer, W.; Gyger, S.; Florian, M.; Lorke, M.; Jahnke, F.; et al. Gate-Switchable Arrays of Quantum Light Emitters in Contacted Monolayer MoS₂ van der Waals Heterodevices. *Nano Lett.* **2021**, *21* (2), 1040–1046.
- (35) Zhou, S.; Guo, X.; Chen, K.; Cole, M. T.; Wang, X.; Li, Z.; Dai, J.; Li, C.; Dai, Q. Optical-Field-Driven Electron Tunneling in Metal-Insulator-Metal Nanojunction. *Advanced Science* **2021**, *8* (24), 2101572.
- (36) Tabe, M.; Terao, Y.; Ishikawa, R.; Asahi, N.; Amemiya, Y. Simulation of Visible Light Induced Effects in a Tunnel Junction Array for Photonic Device Applications. *Jpn. J. Appl. Phys.* **1999**, *38* (1S), 593.
- (37) Choueib, M.; Ayari, A.; Vincent, P.; Bechelany, M.; Cornu, D.; Purcell, S. T. Strong deviations from Fowler-Nordheim behavior for field emission from individual SiC nanowires due to restricted bulk carrier generation. *Phys. Rev. B* **2009**, *79* (7), 075421.
- (38) Laturia, A.; Van de Put, M. L.; Vandenberghe, W. G. Dielectric properties of hexagonal boron nitride and transition metal dichalcogenides: from monolayer to bulk. *npj 2D Materials and Applications* **2018**, *2* (1), 6.
- (39) Robertson, J. High dielectric constant oxides. *European Physical Journal - Applied Physics* **2004**, *28* (3), 265–291.